CpG islands in MyD88 and ASC/PYCARD/TMS1 promoter regions are differentially methylated in head and neck squamous cell carcinoma and primary lung squamous cell carcinoma

Šutić, Maja; Baranašić, Jurica; Kovač Bilić, Lana; Bilić, Mario; Jakovčević, Antonija; Brčić, Luka; Seiwerth, Sven; Jakopović, Marko; Samaržija, Miroslav; Zechner, Ulrich; ...

Source / Izvornik: **Diagnostic Pathology, 2021, 16**

Journal article, Published version
Rad u časopisu, Objavljena verzija rada (izdavačev PDF)

https://doi.org/10.1186/s13000-021-01078-3

Permanent link / Trajna poveznica: https://urn.nsk.hr/urn:nbn:hr:105:184328

Iron overload in aging *Bmp6*$^{-/-}$ mice induces exocrine pancreatic injury and fibrosis due to acinar cell loss

MARTINA PAUK[1], VERA KUFNER[1], VIKTORIJA RUMENOVIC[1], IVO DUMIC-CULE[1,4], VLADIMIR FARKAS[2], MILAN MILOSEVIC[3], TATJANA BORDUKALO-NIKSIC[1] and SLOBODAN VUKICEVIC[1]

[1]Laboratory for Mineralized Tissues, Center for Translational and Clinical Research, School of Medicine, University of Zagreb; [2]Molecular Biology Department, Rudjer Boskovic Institute; [3]Andrija Stampar School of Public Health, School of Medicine, University of Zagreb, HR-10000 Zagreb, Croatia

Received May 26, 2020; Accepted January 19, 2021

DOI: 10.3892/ijmm.2021.4893

Abstract. The relationship between hemochromatosis and diabetes has been well established, as excessive iron deposition has been reported to result in impaired function of the endocrine and exocrine pancreas. Therefore, the objective of the present study was to analyze the effects of iron accumulation on the pancreata and glucose homeostasis in a bone morphogenetic protein 6-knockout (*Bmp6*$^{-/-}$) mouse model of hemochromatosis. The sera and pancreatic tissues of wild-type (WT) and *Bmp6*$^{-/-}$ mice (age, 3 and 10 months) were subjected to biochemical and histological analyses. In addition, ^{18}F-fluorodeoxyglucose biodistribution was evaluated in the liver, muscle, heart, kidney and adipose tissue of both animal groups. The results demonstrated that 3-month-old *Bmp6*$^{-/-}$ mice exhibited iron accumulation preferentially in the exocrine pancreas, with no signs of pancreatic injury or fibrosis. No changes were observed in the glucose metabolism, as pancreatic islet diameter, insulin and glucagon secretion, blood glucose levels and glucose uptake in the liver, muscle and adipose tissue remained comparable with those in the WT mice. Aging *Bmp6*$^{-/-}$ mice presented with progressive iron deposits in the exocrine pancreas, leading to pancreatic degeneration and injury that was characterized by acinar atrophy, fibrosis and the infiltration of inflammatory cells. However, the aging mice exhibited unaltered blood glucose levels and islet structure, normal insulin secretion and moderately increased α-cell mass compared with those in the age-matched WT mice. Additionally, iron overload and pancreatic damage were not observed in the aging WT mice. These results supported a pathogenic role of iron overload in aging *Bmp6*$^{-/-}$ mice leading to iron-induced exocrine pancreatic deficiency, whereas the endocrine pancreas retained normal function.

Correspondence to: Professor Slobodan Vukicevic, Laboratory for Mineralized Tissues, Center for Translational and Clinical Research, School of Medicine, University of Zagreb, 11 Salata Street, HR-10000 Zagreb, Croatia
E-mail: slobodan.vukicevic@mef.hr

Present address: [4]Children's Hospital Srebrnjak, HR-10000 Zagreb, Croatia

Abbreviations: BMP, bone morphogenetic protein; HH, hereditary hemochromatosis; HFE, hemochromatosis protein; Hamp, hepcidin; WT, wild-type; 18-FDG, ^{18}F-fluorodeoxyglucose

Key words: bone morphogenetic protein 6, glucose homeostasis, pancreas, iron metabolism, diabetes

Introduction

Hereditary hemochromatosis (HH) is a heterogeneous group of genetic disorders characterized by the deficiency or dysregulation of the liver hormone hepcidin, a key regulator of systemic iron homeostasis (1). Hepcidin acts via binding to the iron exporter ferroportin, inducing its degradation and subsequently inhibiting intestinal iron absorption and macrophage iron release (2). Insufficient hepcidin production results in excessive iron accumulation in the parenchymal cells of the liver, heart, pancreas and other organs, leading to tissue damage and fibrosis (3). HH is caused by mutations in the genes encoding hemochromatosis protein (HFE), transferrin receptor 2 (Tfr2), hemojuvelin (HJV), ferroportin (SLC40A1) and hepcidin (Hamp); however, for a limited subset of patients with HH-like phenotypes, mutations have been identified in bone morphogenetic protein 6 (BMP6) (4,5).

Bone morphogenetic proteins (BMPs) belong to the transforming growth factor-β (TGF-β) superfamily (6,7) and serve distinct roles in various biological processes, ranging from embryogenesis and development to adult tissue homeostasis (8,9). Our previous studies have reported that the loss of endogenous BMP6 in animal models leads to iron overload and hemochromatosis with low levels of serum hepcidin, suggesting a key role of BMP6 in iron metabolism (10,11). The administration of BMP6 increases hepcidin expression and consequently reduces serum iron levels, whereas BMP inhibitors inhibit hepcidin synthesis, mobilize reticuloendothelial iron cell stores and increase the circulating iron levels (10,12,13).

Although the pathogenesis of diabetes associated with hemochromatosis has not been fully elucidated, it is considered to be multifactorial; it has been suggested that both insulin deficiency and resistance are contributing factors for glucose intolerance and diabetes, which have a high prevalence among

patients with hemochromatosis (14-16). Previous studies on mouse models of HH have demonstrated excessive iron accumulation predominantly in the exocrine pancreas in *Hamp*$^{-/-}$, *HJV*$^{-/-}$, *Bmp6*$^{-/-}$ and *Trf*$^{-/-}$ mice (10,17-21). In aging *Hamp*$^{-/-}$ and *SLC40A1*$^{C326S/C326S}$ mice, iron overload in the pancreatic acinar cells leads to chronic pancreatitis and exocrine pancreatic failure without an effect on glucose homeostasis (22,23). In *HFE*$^{-/-}$ mice, which is another mouse model of hemochromatosis, excess iron in β cells results in pancreatic islet apoptosis, leading to a decrease in insulin secretory capacity and an age-dependent decrease in glucose tolerance, without developing diabetes (24).

Considering the numerous studies on the association between iron metabolism and glucose homeostasis in multiple transgenic mouse lines, the present study aimed to further characterize another mouse model of hemochromatosis. Since *Bmp6*$^{-/-}$ mice exhibit an iron overload phenotype with increased iron accumulation in the liver and pancreas, the present study aimed to analyze glucose homeostasis in *Bmp6*$^{-/-}$ mice and characterize the pathogenic consequences of iron overload on the pancreatic tissue of aging *Bmp6*$^{-/-}$ mice.

Materials and methods

Animals. The use and care of animals used in the present study was in compliance with the standard operating procedures of the animal facility and the European Convention for the Protection of Vertebrate Animals Used for Experimental and Other Scientific Purposes (ETS 123) (25). Animals were housed in conventional laboratory conditions with standard good laboratory practice diet (Mucedola S.R.L.) and water *ad libitum*. *Bmp6*$^{-/-}$ mice with a mixed 129Sv/C57 background were obtained by courtesy of Professor Elisabeth Robertson (University of Oxford, Oxford, UK) (26). Animals were monitored daily for general health and signs of distress or pain, as evidenced by decreased or no appetite, weight loss, little or no movement, or lethargy. Male *Bmp6*$^{-/-}$ mice and background strain-matched wild-type (WT) mice were subjected to analyses at 3 and 10 months of age (n=6 mice/group). After blood sampling, all animals were re-anesthetized and sacrificed by cervical dislocation, and pancreatic tissue samples were collected. The sera and pancreatic tissues were subjected to biochemical and histological analysis, respectively. The present study was approved by the Ethical Committee of The University of Zagreb, Faculty of Sciences (Zagreb, Croatia; approval no. 251-58-508-12-49).

Biochemical parameters. Mice were anesthetized intraperitoneally with a ketamine/xylazine solution (200 mg/kg ketamine and 10 mg/kg xylazine). Blood samples (200-500 μl) were collected from the retro-orbital sinus of the mice using capillary tubes following overnight (16 h) fasting. Within 1 h of collection, the blood samples were centrifuged at 1,000 x g for 15 min at 4˚C for serum separation. The serum was frozen at -80˚C until analysis within 1 week of collection. Blood glucose levels were measured using an Accu-Chek® glucose assay (Roche Diabetes Care, Ltd.). Serum alanine transaminase and aspartate transaminase levels were determined using the Roche Cobas® 6000 clinical chemical analysis machine (F. Hoffmann-La Roche, Ltd.). All original reagents were obtained from Roche Diagnostics. Serum amylase and lipase activity levels were measured as previously described (27).

Histology and immunohistochemistry. Pancreatic tissues from *Bmp6*$^{-/-}$ and WT mice were fixed in 10% formalin at room temperature for 24 h and embedded in paraffin. Sections were cut at 5 μm, deparaffinized in xylene and hydrated in distilled water. To identify morphological changes, the sections were stained with hematoxylin and eosin according to standard methods. To determine the iron levels, the sections were placed in Perl's solution (5% potassium ferrocyanide and 5% HCl) for 30 min at room temperature and counterstained with nuclear fast red (Sigma-Aldrich; Merck KGaA) according to the manufacturer's instructions. For the measurement of collagen deposition, the sections were placed in 0.1% Sirius Red solution (Fluka; Honeywell International, Inc.) dissolved in aqueous saturated 1.2% picric acid, pH 2.0, for 1 h, washed twice with acidified water (0.5% acetic acid) and passed through 100% ethanol thrice using standard procedures. Quantitative analysis of collagen deposition was performed using ImageJ software (version 1.51r; National Institutes of Health) as previously described (28). The amount of collagen was expressed as a percentage of the total pancreatic surface. The pancreatic islet diameter was measured using ImageJ software. For immunohistochemistry, rabbit anti-insulin (cat. no. ab181547; dilution, 1:64,000; Abcam), mouse anti-glucagon (cat. no. sc-71152; dilution 1:25; Santa Cruz Biotechnology, Inc.), mouse anti- macrophage (Clone KiM2R; cat. no. ABIN284638; dilution, 1:40; Antibodies Online) and rabbit anti-CD15 (Clone FUT4/1478R; Novusbio NBP2-53367, dilution 1:10) antibodies were added, and the samples were incubated at 4˚C overnight in a humidified chamber. Micro-polymer IHC Detection kit (cat. no. ab236467; Abcam) was used according to manufacturer's instructions with a goat anti-rabbit secondary antibody incubation for 1 h at room temperature. Images were captured using an Olympus BX51 light microscope (Olympus Corporation) under x10 and x20 magnification. A minimum of five unique fields of view were analyzed per sample of pancreatic tissue obtained from four mice per group.

Small-animal positron emission tomography (PET) study. PET studies were performed with a small animal PET scanner (Raytest ClearPET; Elysia-Raytest GmbH) (29). Briefly, 3-month-old WT and *Bmp6*$^{-/-}$ mice (n=4 mice/group) were injected intraperitoneally with 10-18 MBq ^{18}F-fluorodeoxyglucose (18-FDG) following a short anesthesia period with 200 mg/kg ketamine and 10 mg/kg xylazine. PET was started 60 min after 18-FDG injection. The biodistribution of 18-FDG in the target tissues (heart, quadriceps, liver, kidney, urinary bladder and adipose tissue) was compared between non-fasted WT and *Bmp*$^{-/-}$ mice. After the experiment, the mice were allowed to recover from anesthesia and returned to their cages.

Quantitative image analysis. Regions of interest (ROIs) were manually drawn over the following organs: Liver, heart, kidney, quadriceps, bladder and adipose tissue. The ROIs were applied to the automatically co-registered PET images to measure the corresponding 18-FDG standard uptake value (SUV; mean and maximum). 18-FDG uptake was quantified using the following formula: SUV=tissue activity concentration (Bq/ml)/injected dose (Bq) x body weight (g).

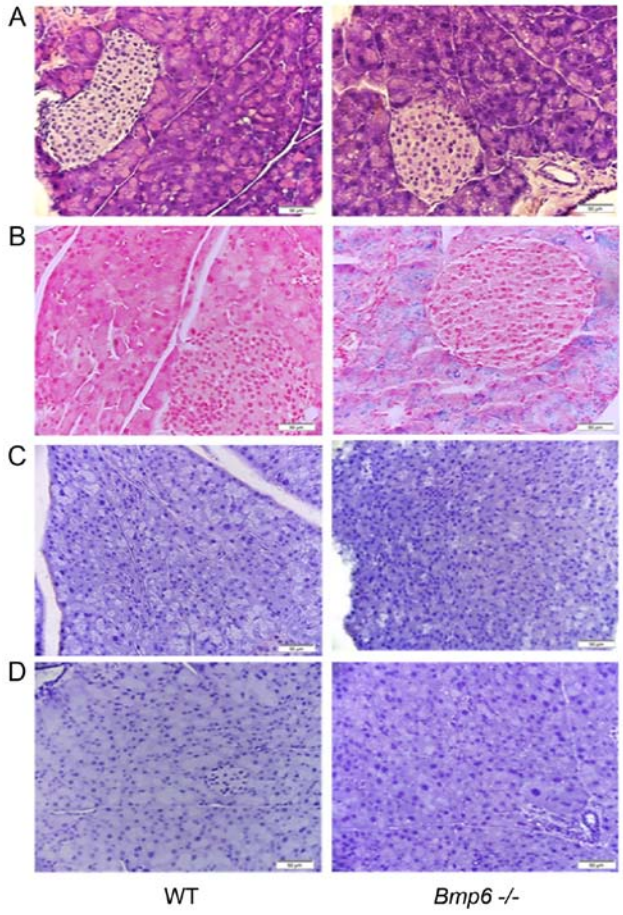

Figure 1. Young *Bmp6*$^{-/-}$ mice exhibit iron overload in the exocrine pancreas with no histological changes. (A-D) Pancreata from 3-month-old WT and *Bmp6*$^{-/-}$ mice (n=6 mice/group) were analyzed for morphological changes by (A) hematoxylin and eosin staining, (B) iron measurement by Perl's Prussian blue staining, (C) degree of pancreatic inflammation by neutrophil marker CD15 and (D) macrophage marker KiM2R immunostaining. Original magnification, x20. Scale bar, 50 μm. *Bmp6*$^{-/-}$, bone morphogenetic protein 6-knockout; WT, wild-type.

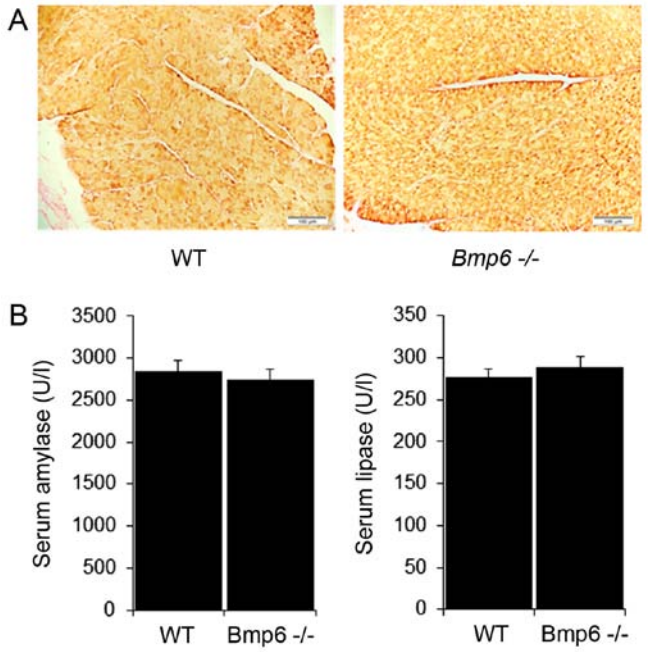

Figure 2. Young *Bmp6*$^{-/-}$ mice exhibit no signs of pancreatic fibrosis. (A) Pancreata from 3-month-old WT and *Bmp6*$^{-/-}$ mice (n=6 mice/group) were analyzed for collagen deposition by Sirius Red staining. Original magnification, x10. Scale bar, 100 μm. (B) Serum amylase and lipase levels were assessed as pancreatic injury markers. Data are presented as the mean ± SD. *Bmp6*$^{-/-}$, bone morphogenetic protein 6-knockout; WT, wild-type.

Statistical analysis. The data are presented as the mean ± standard deviation. Changes in gene expression and serum parameter levels were evaluated using the unpaired two-tailed Student's t-test in Microsoft Office Excel 2016 (Microsoft Corporation). $P<0.05$ was considered to indicate a statistically significant difference.

Results

Young Bmp6$^{-/-}$ *mice present with normal pancreatic parenchyma with iron deposits in the exocrine pancreas*. Pancreatic sections of 3-month-old *Bmp6*$^{-/-}$ mice exhibited normal pancreatic cell morphology (Fig. 1A) and iron deposits in the acinar cells of the exocrine pancreas, whereas no iron accumulation was observed in the pancreatic islets (Fig. 1B). WT and *Bmp6*$^{-/-}$ mice exhibited no signs of inflammatory processes in the pancreas, as the accumulation of the macrophage marker KiM2R and the neutrophil marker CD15 was not observed by immunohistochemistry (Fig. 1C and D). Further examination of the pancreatic tissues in *Bmp6*$^{-/-}$ mice revealed no signs of fibrosis, as demonstrated by the absence of collagen fibers and similar levels of the pancreatic enzymes amylase and lipase compared with those in WT mice (Fig. 2A and B). Taken together, these results demonstrated that iron overload did not induce any morphological alterations of the exocrine pancreas in 3-month-old *Bmp6*$^{-/-}$ mice.

Young Bmp6$^{-/-}$ *mice exhibit normal morphology and function of the endocrine pancreas*. The effects of iron overload on glucose homeostasis were next analyzed in 3-month-old *Bmp6*$^{-/-}$ mice. The blood glucose levels did not differ between *Bmp6*$^{-/-}$ and WT mice (Fig. 3A). Morphometric analysis of pancreatic sections revealed no significant differences in the mean diameter of pancreatic islets compared with that in the WT mice (Fig. 3B). Immunohistochemical staining also demonstrated no changes in the distribution of β insulin cells and insulin content (Fig. 3C). In addition, glucagon-stained sections revealed no significant changes in the number or distribution of α-cells located in the periphery of the islets in *Bmp6*$^{-/-}$ and WT mice (Fig. 3D). To determine the potential differences in the biodistribution of glucose, tissue uptake of 18-FDG was evaluated in *Bmp6*$^{-/-}$ and WT mice. With the exception of increased 18-FDG uptake in the bladders of *Bmp6*$^{-/-}$ mice compared with that in WT mice, no significant differences in 18-FDG uptake were observed in the liver, muscle, heart, kidney and adipose tissues between the two groups (Fig. 3E). These results suggested that iron overload in the exocrine pancreas did not affect the viability and function of the endocrine pancreas in 3-month-old *Bmp6*$^{-/-}$ mice.

Aging Bmp6$^{-/-}$ *mice develop morphologic alterations in the exocrine pancreas due to iron overload*. Pancreatic sections from aging WT mice presented with morphologically normal islets surrounded by exocrine pancreatic tissue without iron

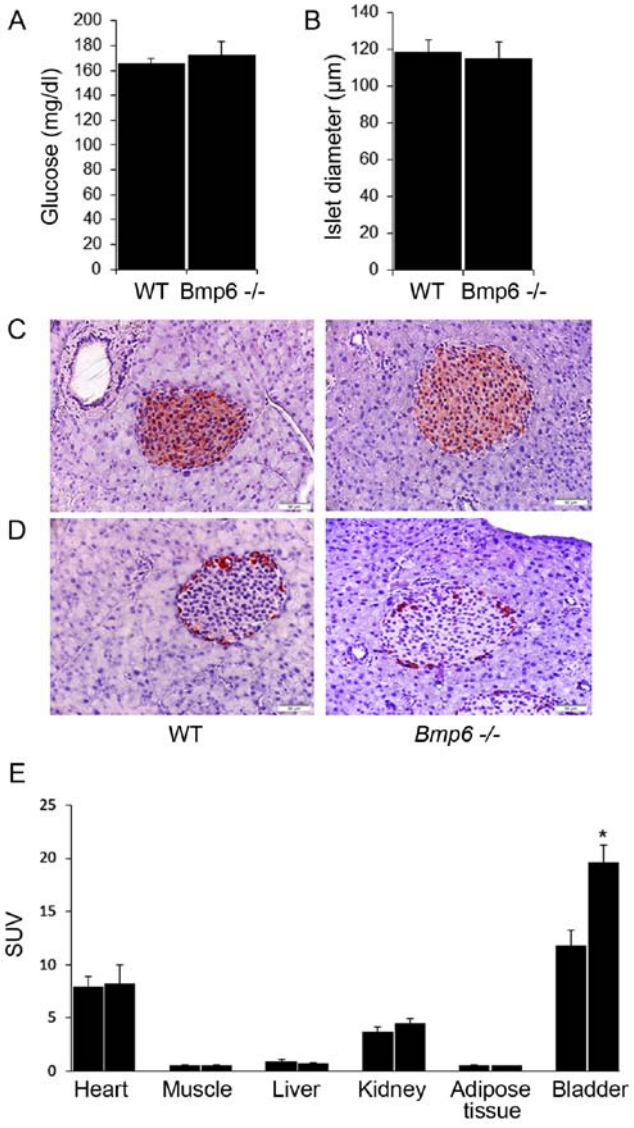

Figure 3. Young *Bmp6*$^{-/-}$ mice exhibit normal glucose metabolism. (A) Blood glucose levels were measured following overnight fasting in 3-month-old WT and *Bmp6*$^{-/-}$ mice (n=6 mice/group). (B-D) Pancreatic sections were analyzed for (B) mean diameter of pancreatic islets, (C) insulin and (D) glucagon secretion by immunohistochemistry. Original magnification, x20. Scale bar, 50 μm. (E) Biodistribution of 18-FDG in target tissues was assessed 60 min post-i.p. injection of 10-18 MBq 18-FDG (n=4 mice/group). 18-FDG uptake was expressed as SUV. Data are presented as the mean ± SD. *P<0.05 vs. WT. *Bmp6*$^{-/-}$, bone morphogenetic protein 6-knockout; WT, wild-type; 18-FDG, ^{18}F-fluorodeoxyglucose; SUV, standardized uptake value.

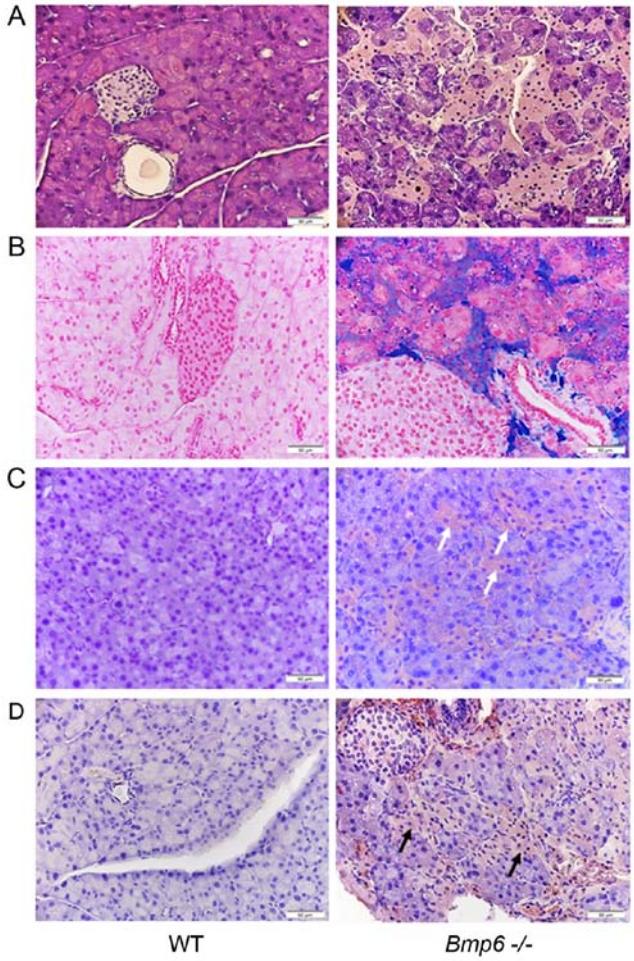

Figure 4. Aging *Bmp6*$^{-/-}$ mice exhibit severe iron overload in the exocrine pancreas, leading to acinar cell loss and macrophage infiltration. (A-D) Pancreata from 10-month-old WT and *Bmp6*$^{-/-}$ mice (n=6 mice/group) were analyzed for (A) morphological changes by hematoxylin and eosin staining, (B) iron measurement by Perl's Prussian blue staining, (C) degree of pancreatic inflammation by neutrophil marker CD15 (white arrows) and (D) macrophage marker KiM2R (black arrows) immunostaining. Original magnification, x20. Scale bar, 50 μm. *Bmp6*$^{-/-}$, bone morphogenetic protein 6-knockout; WT, wild-type.

deposits (Fig. 4A and B). By contrast, histological analysis of 10-month-old *Bmp6*$^{-/-}$ mice demonstrated marked iron deposits in the exocrine pancreas, which were associated with pancreatic atrophy due to pronounced degeneration of the pancreatic acini (Fig. 4A and B). Morphological alterations included the shrinkage of numerous acinar cells with cytoplasmic loss of zymogen granules compared with the WT controls. In addition, the acinar cells were randomly distributed across the entire pancreas without a particular pattern. Consistent with the acinar cell loss, immunohistochemical staining revealed that the neutrophil marker CD15 (Fig. 4C) and the macrophage marker KiM2R (Fig. 4D) were present in the pancreatic tissues of *Bmp6*$^{-/-}$ mice. In addition, aging *Bmp6*$^{-/-}$ mice developed pancreatic fibrosis with collagen distribution in the interlobular and periacinar areas and around the pancreatic ducts (Fig. 5A). In aging WT mice, collagen was observed around the pancreatic ducts and blood vessels. These fibrogenic changes were quantified by morphometric analysis, which confirmed a marked increase in the pancreatic collagen deposition in aging *Bmp6*$^{-/-}$ mice compared with that in the WT mice (Fig. 5B). However, no significant differences were observed in serum amylase and lipase levels between aging WT and *Bmp6*$^{-/-}$ mice (Fig. 5C). Serum alanine transaminase and aspartate transaminase, blood markers of liver function, also did not differ between WT and *Bmp6*$^{-/-}$ mice at 3 and 10 months (Fig. S1). Iron overload and consequent exocrine pancreatic damage were not observed in aging WT mice. These results suggested that iron loading in aging *Bmp6*$^{-/-}$ mice led to exocrine pancreatic injury and fibrosis, as revealed by acinar cell loss, inflammatory cell infiltration and collagen deposition in the pancreas.

Aging Bmp6$^{-/-}$ *mice display normal morphology and function of the endocrine pancreas*. The effects of exocrine pancreatic damage on the endocrine pancreas were further evaluated in

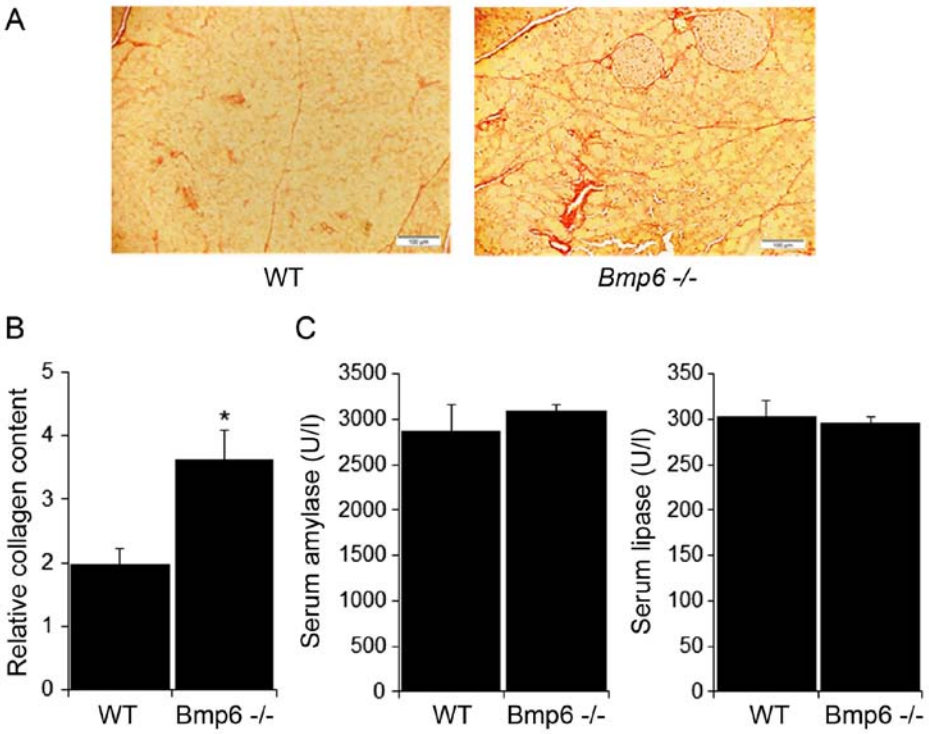

Figure 5. Aging *Bmp6*$^{-/-}$ mice develop pancreatic fibrosis. (A and B) Pancreata from 10-month-old WT and *Bmp6*$^{-/-}$ mice (n=6 mice/group) were analyzed for (A) collagen deposition by Sirius Red staining and (B) relative amount of pancreatic collagen quantified by morphometric analysis. Original magnification, x10. Scale bar, 100 μm. (C) Serum amylase and lipase levels were assessed as pancreatic injury markers. Data are presented as the mean ± SD. *P<0.05 vs. WT. *Bmp6*$^{-/-}$, bone morphogenetic protein 6-knockout; WT, wild-type.

aging *Bmp6*$^{-/-}$ mice. No significant differences were observed in the blood glucose levels between aging WT and *Bmp6*$^{-/-}$ mice (Fig. 6A). The mean diameter of pancreatic islets in *Bmp6*$^{-/-}$ mice was comparable with that in the WT control (Fig. 6B). In addition, pancreatic sections from aging *Bmp6*$^{-/-}$ mice appeared to exhibit normal islet architecture and a similar staining pattern for insulin (Fig. 6C), with the exception of moderately increased glucagon-positive area (Fig. 6D) compared with that in the WT mice. Collectively, despite acinar cell death and atrophy of the exocrine pancreas, no morphological neither functional impairment was observed on the endocrine pancreas in aging *Bmp6*$^{-/-}$ mice.

Discussion

Over the past 10 years, there has been a focus on understanding the role of iron in the pathogenesis of diabetes (30). The mechanisms by which iron contributes to diabetes have not been fully elucidated. Excess iron in the liver is considered to interfere with glucose metabolism leading to insulin resistance, whereas pancreatic iron loading results in β-cell damage and reduced insulin secretion (14-16). The prevalence of diabetes in patients with HH has been reported to be 7-40% (14,31), with abnormal glucose tolerance detected in 30% of patients with HH compared with that in healthy subjects (14,32). To further understand the role of iron in diabetes, the present study characterized an animal model of hemochromatosis using *Bmp6*$^{-/-}$ mice.

Misexpression of BMP6 has been previously reported to lead to agenesis of the pancreas and a reduction in the size of the stomach and the spleen, causing fusion of the liver and duodenum (33). Our previous studies have demonstrated that *Bmp6*$^{-/-}$ mice present with a phenotype resembling HH, with low levels of hepcidin expression and iron overload, suggesting a key role of BMP6 in iron metabolism (10,11,20). The results of the present study demonstrated that iron overload in *Bmp6*$^{-/-}$ mice led to a marked increase of iron content in the exocrine pancreatic tissue and induced morphologic alterations of the pancreas during aging. Although these animals exhibited iron accumulation in pancreatic acinar cells at 3 months, progressive iron deposits associated with severe tissue degeneration were noticeable at 10 months. Aging *Bmp6*$^{-/-}$ mice developed severe pancreatic fibrosis, which was revealed by increased deposition of collagen compared with that in the age-matched WT mice. This was accompanied with pancreatic atrophy and macrophage recruitment, suggesting that macrophages may be involved in clearing apoptotic cells following injury. By contrast, iron overload, inflammatory reaction and pancreatic damage were not observed in aging WT mice.

In the present study, *Bmp6*$^{-/-}$ mice did not exhibit any signs of liver damage, as serum levels of alanine transaminase and aspartate transaminase, which are markers of liver metabolism (34), did not differ between the WT and *Bmp6*$^{-/-}$ mice in either age group. Previous studies in *Bmp6*$^{-/-}$ mice have reported the existence of distinct regulatory mechanisms that sense hepatic iron in order to stimulate expression of hepcidin, the main regulator of iron metabolism (20,35). BMP2 has also been demonstrated to be able to replace BMP6, activate Smad1/5/8 phosphorylation and significantly induce hepcidin expression *in vivo* (18,36). In addition to BMP6, another suitable candidate for hepcidin regulation is BMP2, the dominant BMP ligand expressed in liver endothelial cells that stimulates hepcidin *in vivo* (36,37). The important role of BMP2 in

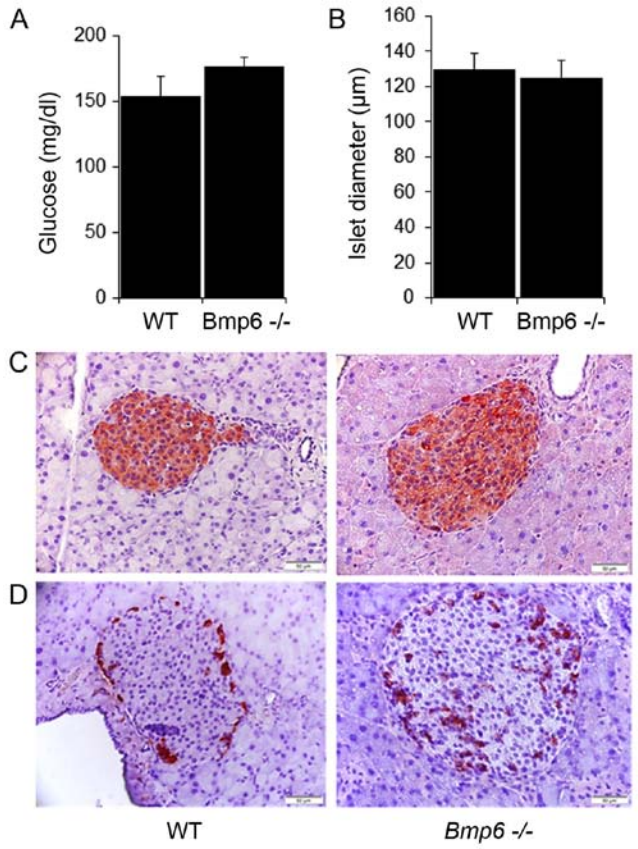

Figure 6. Damaged exocrine pancreas does not affect glucose metabolism in aging *Bmp6*$^{-/-}$ mice. (A) Blood glucose levels were measured following overnight fasting in 10-month-old WT and *Bmp6*$^{-/-}$ mice (n=6 mice/group). (B-D) Pancreatic sections were analyzed for (B) mean diameter of pancreatic islets, (C) insulin and (D) glucagon secretion by immunohistochemistry. Original magnification, x20. Scale bar, 50 μm. Data are presented as the mean ± SD. *Bmp6*$^{-/-}$, bone morphogenetic protein 6-knockout; WT, wild-type.

hepcidin regulation has been confirmed in mice with a conditional knockout of BMP2, which exhibit a hemochromatosis phenotype similar to that observed in *Bmp6*$^{-/-}$ mice (36). Furthermore, similar hepatocellular iron overload without developing liver fibrosis has also been reported in other mouse models of HH such as *HFE*$^{-/-}$, *SLC40A1*$^{C326S/C326S}$, *Hamp*$^{-/-}$ and *Hjv*$^{-/-}$ mice (22,23,38,39). *Hjv*$^{-/-}$ mice have been demonstrated to be resistant to liver fibrosis even after consuming a high-fat diet supplemented with iron (40). The livers of *Hamp*$^{-/-}$ mice exhibit low mRNA levels of divalent metal transporter 1 (*DMT1*) and *Tfr1*, which mediate the uptake of non-transferrin-bound and transferrin-bound iron, respectively (23). By contrast, the *DMT1* mRNA levels are slightly increased in *Hamp*-knockout pancreata compared with those in pancreatic tissues from WT animals, suggesting that *Hamp*$^{-/-}$ mice have a transcriptional response promoting iron uptake in the pancreas. Other studies on HH mouse models, such as *HFE*$^{-/-}$, *SLC40A1*$^{C326S/C326S}$ and *Hjv*$^{-/-}$ mice, have concluded that despite severe tissue iron overload, these mice are protected from liver damage by yet unknown mechanisms (22,38-40). Further studies should clarify whether hepatic iron regulation in *Bmp6*$^{-/-}$ mice is modulated by other BMP ligands or other mechanisms, including transcriptional responses of iron transporters. The results of the present study were in accordance with those of previous studies (10,17-20), in which malfunctions of the hepcidin-ferroportin regulatory axis contributed to iron accumulation in the exocrine pancreas. Similar sensitivity of the exocrine pancreas to iron overload has been observed in mice with a ferroportin mutation (*SLC40A1*$^{C326S/C326S}$), where pancreatic failure leads to premature death between 7 and 14 months of age (22). These mice display profound weight loss attributed to malabsorption as a result of exocrine pancreatic insufficiency and a lack of digestive enzymes (22). Compared with these mice, *Hamp*$^{-/-}$ mice exhibit iron overload-induced chronic pancreatitis, but the pancreatic damage is not associated with any changes in serum lipase levels or premature lethality (23). Chronic pancreatitis is characterized by inflammatory cell infiltration, acinar cell degeneration and development of fibrosis, which may lead to the impairment of exocrine and endocrine pancreatic function (41). In the present study, following the progression of acinar cell damage, 10-month-old *Bmp6*$^{-/-}$ mice exhibited no changes in serum amylase and lipase levels compared with those in the WT mice, suggesting limited acinar damage that was not reflected by histological changes. In addition, these mice had a normal lifespan without exhibiting any weight loss or diarrhea (data not shown), suggesting that the extent of pancreatic injury and acinar cell loss was not sufficient for iron-mediated lethality. Further studies are needed to investigate why these differences in mortality occur among mouse models of hemochromatosis with similar patterns of iron deposition and consequent exocrine pancreatic insufficiency.

As demonstrated by acinar cell loss, fibrosis and infiltration of inflammatory cells, the exocrine pancreas in *Bmp6*$^{-/-}$ mice was severely affected in the present study. Our recent study indicated the possible role of BMP6 in glucose homeostasis (42). The role of BMP6 in development of diabetes, although reported in the literature, is still not fully understood. Recently, delayed fracture healing due to the BMP6 downregulation has been reported in a streptozotocin-induced rat diabetes model (43). The low *Bmp6* expression levels in smooth muscle progenitor cells in a mouse diabetes model (44) and in myofibroblast progenitor cells of patients with diabetes (45) has suggested the role of BMP6 in vascular tissue remodeling, which may promote the generation of cells with antiangiogenic and profibrotic properties (46). The present study aimed to investigate whether exocrine pancreatic damage may impact glucose metabolism in aging *Bmp6*$^{-/-}$ mice. The islet diameters in *Bmp6*$^{-/-}$ and WT mice were similar during aging, suggesting no changes in β-cell mass. In addition, no changes were observed in the insulin content by immunohistochemistry in the pancreatic tissues during aging in both animal groups. Blood glucose levels and 18-FDG uptake in the liver, muscle and adipose tissues were comparable in *Bmp6*$^{-/-}$ and WT mice, suggesting normal glucose metabolism. By contrast, aging *Bmp6*$^{-/-}$ mice exhibited moderately increased islet glucagon content compared with that in the WT mice, indicating increased α-cell mass. The role of altered glucagon content in aging *Bmp6*$^{-/-}$ mice should be additionally studied in animals >10 months.

HFE$^{-/-}$ mice exhibit iron accumulation in β cells, resulting in decreased insulin secretion compared with that in WT animals, secondary to β cell oxidant stress and apoptosis without developing diabetes (24). However, other mouse models of HH such as *Hamp*$^{-/-}$ and *Hjv*$^{-/-}$ mice present with preferential iron loading in the exocrine pancreas without impacting β cells and glucose homeostasis (17,38). *SLC40A1*$^{C326S/C326S}$ mice also

display excessive iron accumulation in the pancreatic acinar cells but differ from the other models by failure of the exocrine pancreas (22). Despite degeneration of the pancreatic acini, aged *Hamp*$^{-/-}$ mice exhibit normal glucose homeostasis (17). A previous study has suggested an important role of zinc transporter ZIP14, a member of the ZIP family of metal ion transporters, in contributing to non-transferrin-bound iron uptake and iron accumulation by hepatocytes and pancreatic acinar cells in iron overload disorders (47). Since *DMT1* and *Tfr1* expression levels are low in *SLC40A1*$^{C326S/C326S}$ mice, iron accumulation in the exocrine pancreas may be attributed to the increased uptake of non-transferrin-bound iron via ZIP14 (22). In addition, *SLC40A1*$^{C326S/C326S}$ mice present with a subset of acinar cells that lack ferroportin expression, which may be prone to extensive iron accumulation and degeneration (22). Additionally, *Hamp*$^{-/-}$ mice exhibit the same pattern of ferroportin expression in the pancreas (23). Although the endocrine pancreas of *Hamp*$^{-/-}$ mice contains high levels of ferroportin, a limited number of acinar cells that undergo severe iron overload have relatively low ferroportin levels; however, it remains unclear why a number of the acinar cells do not express ferroportin, and whether this may be the reason for preferential iron accumulation in the exocrine pancreas in these animals (23). Notably, *SLC40A1*$^{C326S/C326S}$ and *Hamp*$^{-/-}$ mice exhibit high hepatic levels of *Bmp6* mRNA and a functional BMP/SMAD signaling pathway (48,49), indicating that acinar cell loss leading to exocrine pancreatic injury in these mice is a direct effect of iron loading and is not attributed to any effects of BMP6.

The present study had certain limitations. The results of the study are preliminary, as only two age groups of mice were evaluated. To further understand the glucose metabolism of *Bmp6*$^{-/-}$ mice, glucose and insulin tolerance tests, as well as analysis of serum insulin and glucagon levels will be performed in future studies. In addition, more age groups, in particular mice >10 months, may provide further insight into the changes in the pancreas and other organs in this animal model during aging.

In conclusion, the results of the present study demonstrated that *Bmp6*$^{-/-}$ mice exhibited features of chronic pancreatitis due to age-dependent iron accumulation in the exocrine pancreas. However, acinar cell atrophy and exocrine pancreatic injury did not induce diabetes in *Bmp6*$^{-/-}$ mice, as these animals exhibited normal islet structure with unaltered levels of insulin production and blood glucose. Future studies are needed to determine why iron predominately accumulated in the exocrine pancreas and thereby protected pancreatic islets against iron accumulation and oxidative damage in *Bmp6*$^{-/-}$ mice.

Acknowledgements

The authors would like to thank Mrs. Djurdjica Car and Mrs. Mirjana Marija Renic (University of Zagreb, Zagreb, Croatia) for their technical support in animal experiments.

Funding

The present study was supported by the Scientific Center of Excellence for Reproductive and Regenerative Medicine (project 'Reproductive and regenerative medicine-exploration of new platforms and potentials'; grant. no. GA KK.01.1.1.01.0008) funded by the EU through the ERDF.

Availability of data and materials

All data generated or analyzed during this study are included in this published article.

Authors' contributions

MP and SV conceived the study and designed the methodology. MP, VK, VR, IDC, VF, MM and TBN performed the experiments and analyzed the data. MP wrote the original draft. MP, VK, TBN and SV revised the manuscript. SV acquired the funding and supervised the study. MP, TBN and SV confirm the authenticity of all the raw data. All authors read and approved the final manuscript.

Ethics approval and consent to participate

All applicable international, national, and/or institutional guidelines for the care and use of animals were followed. The present study was approved by the Ethical Committee of The University of Zagreb, Faculty of Sciences (Zagreb, Croatia; approval no. 251-58-508-12-49).

Patient consent for publication

Not applicable.

Competing interests

The authors declare that they have no competing interests.

References

1. Fleming RE and Ponka P: Iron overload in human disease. N Engl J Med 366: 348-359, 2012.
2. Nemeth E, Tuttle MS, Powelson J, Vaughn MB, Donovan A, Ward DM, Ganz T and Kaplan J: Hepcidin regulates cellular iron efflux by binding to ferroportin and inducing its internalization. Science 306: 2090-2093, 2004.
3. Pietrangelo A: Hereditary hemochromatosis: Pathogenesis, diagnosis, and treatment. Gastroenterology 139: 393-408, 408. e1-e2, 2010.
4. Piubelli C, Castagna A, Marchi G, Rizzi M, Busti F, Badar S, Marchetti M, De Gobbi M, Roetto A, Xumerle L, *et al*: Identification of new BMP6 pro-peptide mutations in patients with iron overload. Am J Hematol 92: 562-568, 2017.
5. Daher R, Kannengiesser C, Houamel D, Lefebvre T, Bardou-Jacquet E, Ducrot N, de Kerguenec C, Jouanolle AM, Robreau AM, Oudin C, *et al*: Heterozygous mutations in BMP6 pro-peptide lead to inappropriate hepcidin synthesis and moderate iron overload in humans. Gastroenterology 150: 672-683,e4, 2016.
6. Urist MR: Bone: Formation by autoinduction. Science 150: 893-899, 1965.
7. Reddi AH: Role of morphogenetic proteins in skeletal tissue engineering and regeneration. Nat Biotechnol 16: 247-252, 1998.
8. Wagner DO, Sieber C, Bhushan R, Börgermann JH, Graf D and Knaus P: BMPs: From bone to body morphogenetic proteins. Sci Signal 3: mr1, 2010.
9. Sampath KT: The systems biology of bone morphogenetic proteins. In: Bone Morphogenetic Proteins: Systems Biology Regulators. Vukicevic S and Sampath KT (eds). Springer International Publishing, pp15-38, 2017.
10. Andriopoulos B Jr, Corradini E, Xia Y, Faasse SA, Chen S, Grgurevic L, Knutson MD, Pietrangelo A, Vukicevic S, Lin HY and Babitt JL: BMP6 is a key endogenous regulator of hepcidin expression and iron metabolism. Nat Genet 41: 482-487, 2009.
11. Meynard D, Kautz L, Darnaud V, Canonne-Hergaux F, Coppin H and Roth MP: Lack of the bone morphogenetic protein BMP6 induces massive iron overload. Nat Genet 41: 478-481, 2009.

12. Corradini E, Schmidt PJ, Meynard D, Garuti C, Montosi G, Chen S, Vukicevic S, Pietrangelo A, Lin HY and Babitt JL: BMP6 treatment compensates for the molecular defect and ameliorates hemochromatosis in Hfe knockout mice. Gastroenterology 139: 1721-1729, 2010.
13. Yu PB, Hong CC, Sachidanandan C, Babitt JL, Deng DY, Hoyng SA, Lin HY, Bloch KD and Peterson RT: Dorsomorphin inhibits BMP signals required for embryogenesis and iron metabolism. Nat Chem Biol 4: 33-41, 2008.
14. McClain DA, Abraham D, Rogers J, Brady R, Gault P, Ajioka R and Kushner JP: High prevalence of abnormal glucose homeostasis secondary to decreased insulin secretion in individuals with hereditary haemochromatosis. Diabetologia 49: 1661-1669, 2006.
15. Mendler MH, Turlin B, Moirand R, Jouanolle AM, Sapey T, Guyader D, Le Gall JY, Brissot P, David V and Deugnier Y: Insulin resistance-associated hepatic iron overload. Gastroenterology 117: 1155-1163, 1999.
16. Hramiak IM, Finegood DT and Adams PC: Factors affecting glucose tolerance in hereditary hemochromatosis. Clin Invest Med 20: 110-118, 1997.
17. Ramey G, Faye A, Durel B, Viollet B and Vaulont S: Iron overload in Hepc1(-/-) mice is not impairing glucose homeostasis. FEBS Lett 581: 1053-1057, 2007.
18. Latour C, Besson-Fournier C, Meynard D, Silvestri L, Gourbeyre O, Aguilar-Martinez P, Schmidt PJ, Fleming MD, Roth MP and Coppin H: Differing impact of the deletion of hemochromatosis-associated molecules HFE and transferrin receptor-2 on the iron phenotype of mice lacking bone morphogenetic protein 6 or hemojuvelin. Hepatology 63: 126-137, 2016.
19. Latour C, Besson-Fournier C, Gourbeyre O, Meynard D, Roth MP and Coppin H: Deletion of BMP6 worsens the phenotype of HJV-deficient mice and attenuates hepcidin levels reached after LPS challenge. Blood 130: 2339-2343, 2017.
20. Pauk M, Grgurevic L, Brkljacic J, Kufner V, Bordukalo-Niksic T, Grabusic K, Razdorov G, Rogic D, Zuvic M, Oppermann H, *et al*: Exogenous BMP7 corrects plasma iron overload and bone loss in Bmp6-/- mice. Int Orthop 39: 161-172, 2015.
21. Meynard D, Vaja V, Sun CC, Corradini E, Chen S, López-Otín C, Grgurevic L, Hong CC, Stirnberg M, Gütschow M, *et al*: Regulation of TMPRSS6 by BMP6 and iron in human cells and mice. Blood 118: 747-756, 2011.
22. Altamura S, Kessler R, Gröne HJ, Gretz N, Hentze MW, Galy B and Muckenthaler MU: Resistance of ferroportin to hepcidin binding causes exocrine pancreatic failure and fatal iron overload. Cell Metab 20: 359-367, 2014.
23. Lunova M, Schwarz P, Nuraldeen R, Levada K, Kuscuoglu D, Stützle M, Vujić Spasić M, Haybaeck J, Ruchala P, Jirsa M, *et al*: Hepcidin knockout mice spontaneously develop chronic pancreatitis owing to cytoplasmic iron overload in acinar cells. J Pathol 241: 104-114, 2017.
24. Cooksey RC, Jouihan HA, Ajioka RS, Hazel MW, Jones DL, Kushner JP and McClain DA: Oxidative stress, beta-cell apoptosis, and decreased insulin secretory capacity in mouse models of hemochromatosis. Endocrinology 145: 5305-5312, 2004.
25. Council of Europe: European Convention for the Protection of Vertebrate Animals used for Experimental and Other Scientific Purposes. ETS 123, Strasbourg, 1986.
26. Solloway MJ, Dudley AT, Bikoff EK, Lyons KM, Hogan BL and Robertson EJ: Mice lacking Bmp6 function. Dev Genet 22: 321-339, 1998.
27. Bhatia M, Saluja AK, Hofbauer B, Frossard JL, Lee HS, Castagliuolo I, Wang CC, Gerard N, Pothoulakis C and Steer ML: Role of substance P and the neurokinin 1 receptor in acute pancreatitis and pancreatitis-associated lung injury. Proc Natl Acad Sci USA 95: 4760-4765, 1998.
28. Rangan GK and Tesch GH: Quantification of renal pathology by image analysis. Nephrology (Carlton) 12: 553-558, 2007.
29. Roldan PS, Chereul E, Dietzel O, Magnier L, Pautrot C, Rbah-Vidal L, Sappey-Marinier D, Wagner A Zimmer L, Janier MF, *et al*: Raytest ClearPET (TM), a new generation small animal PET scanner. Nucl Instrum Methods Phys Res A Accel Spectrom Detect Assoc Equip 571: 498-501, 2007.
30. Hansen JB, Moen IW and Mandrup-Poulsen T: Iron: The hard player in diabetes pathophysiology. Acta Physiol (Oxf) 210: 717-732, 2014.
31. Buysschaert M, Paris I, Selvais P and Hermans MP: Clinical aspects of diabetes secondary to idiopathic haemochromatosis in French-speaking Belgium. Diabetes Metab 23: 308-313, 1997.
32. Hatunic M, Finucane FM, Brennan AM, Norris S, Pacini G and Nolan JJ: Effect of iron overload on glucose metabolism in patients with hereditary hemochromatosis. Metabolism 59: 380-384, 2010.
33. Dichmann DS, Miller CP, Jensen J, Scott Heller R and Serup P: Expression and misexpression of members of the FGF and TGFbeta families of growth factors in the developing mouse pancreas. Dev Dyn 226: 663-674, 2003.
34. Pratt DS and Kaplan MM: Evaluation of abnormal liver-enzyme results in asymptomatic patients. N Engl J Med 342: 1266-1271, 2000.
35. Ramos E, Kautz L, Rodriguez R, Hansen M, Gabayan V, Ginzburg Y, Roth MP, Nemeth E and Ganz T: Evidence for distinct pathways of hepcidin regulation by acute and chronic iron loading in mice. Hepatology 53: 1333-1341, 2011.
36. Canali S, Wang CY, Zumbrennen-Bullough KB, Bayer A and Babitt JL: Bone morphogenetic protein 2 controls iron homeostasis in mice independent of Bmp6. Am J Hematol 92: 1204-1213, 2017.
37. Xiao X, Dev S, Canali S, Bayer A, Xu Y, Agarwal A, Wang CY and Babitt JL: Endothelial bone morphogenetic protein 2 (Bmp2) knockout exacerbates hemochromatosis in homeostatic iron regulator (Hfe) knockout mice but not bmp6 knockout mice. Hepatology 72: 642-655, 2020.
38. Huang FW, Pinkus JL, Pinkus GS, Fleming MD and Andrews NC: A mouse model of juvenile hemochromatosis. J Clin Invest 115: 2187-2191, 2005.
39. Wagner J, Fillebeen C, Haliotis T, Charlebois E, Katsarou A, Mui J, Vali H and Pantopoulos K: Mouse models of hereditary hemochromatosis do not develop early liver fibrosis in response to a high fat diet. PLoS One 14: e0221455, 2019.
40. Padda RS, Gkouvatsos K, Guido M, Mui J, Vali H and Pantopoulos K: A high-fat diet modulates iron metabolism but does not promote liver fibrosis in hemochromatotic Hjv$^{-/-}$ mice. Am J Physiol Gastrointest Liver Physiol 308: G251-G261, 2015.
41. Mareninova OA, Sung KF, Hong P, Lugea A, Pandol SJ, Gukovsky I and Gukovskaya AS: Cell death in pancreatitis: Caspases protect from necrotizing pancreatitis. J Biol Chem 281: 3370-3381, 2006.
42. Pauk M, Bordukalo-Niksic T, Brkljacic J, Paralkar VM, Brault AL, Dumic-Cule I, Borovecki F, Grgurevic L and Vukicevic S: A novel role of bone morphogenetic protein 6 (BMP6) in glucose homeostasis. Acta Diabetol 56: 365-371, 2019.
43. Guo Q, Wang W, Abboud R and Guo Z: Impairment of maturation of BMP-6 (35 kDa) correlates with delayed fracture healing in experimental diabetes. J Orthop Surg Res 15: 186, 2020.
44. Westerweel PE, van Velthoven CT, Nguyen TQ, den Ouden K, de Kleijn DP, Goumans MJ, Goldschmeding R and Verhaar MC: Modulation of TGF-β/BMP-6 expression and increased levels of circulating smooth muscle progenitor cells in a type I diabetes mouse model. Cardiovasc Diabetol 9: 55, 2010.
45. Nguyen TQ, Chon H, van Nieuwenhoven FA, Braam B, Verhaar MC and Goldschmeding R: Myofibroblast progenitor cells are increased in number in patients with type 1 diabetes and express less bone morphogenetic protein 6: A novel clue to adverse tissue remodelling? Diabetologia 49: 1039-1048, 2006.
46. Vinci MC, Gambini E, Bassetti B, Genovese S and Pompilio G: When good guys turn bad: Bone marrow's and hematopoietic stem cells' role in the pathobiology of diabetic complications. Int J Mol Sci 21: 3864, 2020.
47. Jenkitkasemwong S, Wang CY, Coffey R, Zhang W, Chan A, Biel T, Kim JS, Hojyo S, Fukada T and Knutson MD: SLC39A14 is required for the development of hepatocellular iron overload in murine models of hereditary hemochromatosis. Cell Metab 22: 138-150, 2015.
48. Kautz L, Meynard D, Monnier A, Darnaud V, Bouvet R, Wang RH, Deng C, Vaulont S, Mosser J, Coppin H and Roth MP: Iron regulates phosphorylation of Smad1/5/8 and gene expression of Bmp6, Smad7, Id1, and Atoh8 in the mouse liver. Blood 112: 1503-1509, 2008.
49. Vujić Spasić M, Sparla R, Mleczko-Sanecka K, Migas MC, Breitkopf-Heinlein K, Dooley S, Vaulont S, Fleming RE and Muckenthaler MU: Smad6 and Smad7 are co-regulated with hepcidin in mouse models of iron overload. Biochim Biophys Acta 1832: 76-84, 2013.